Chinese Journal of
POLYMER SCIENCE

RESEARCH ARTICLE

https://doi.org/10.1007/s10118-026-3756-9
Chinese J. Polym. Sci.

Liquid Crystal-driven Superspreading of Polymer Droplets at the Air-Water Interface

Yuan-Zhu Song, Xing-Chao Chen, Yan-Jun Liu*, and Pei-Yi Wu*

State Key Laboratory of Advanced Fiber Materials, College of Chemistry and Chemical Engineering, Center for Advanced Low-Dimension Materials, Donghua University, Shanghai 201620, China

Electronic Supplementary Information

Abstract Ultrathin polymer films are difficult to fabricate over large areas and transfer without damage. Spreading polymer droplets on water offers an atomically flat and releasable substrate, but the attainable area is limited by interfacial friction and tension gradient difference. Here, we show that interfacial resistance, rather than tension difference alone, dictates the spreading limit. By introducing a hydrophobic liquid crystal (4-cyano-4′-heptylbiphenyl, 7CB), we uncover a superspreading phenomenon in which polymer droplets rapidly expand into large-area ultrathin films on aqueous salt solutions. This behavior is enabled by a phase-transition-enabled interfacial lubrication mechanism. During spreading, 7CB reaches a low-mobility nematic liquid-crystalline state and becomes enriched on the organic side of the solvent-water interface, forming a dynamically generated lubricating region that reduces resistance to rapid liquid-liquid spreading. Low-field nuclear magnetic resonance (NMR) measurements reveal a sharp transition in molecular mobility, directly linking the phase state of 7CB to interfacial resistance reduction. This strategy is universal across polymers with diverse mechanical properties and enables the fabrication of transferable, nanometer-thick films with integrated functionalities. These findings redefine the role of liquid-liquid interfaces in spreading dynamics and provide a general framework for designing near-frictionless interfacial transport processes.

Keywords Liquid crystals; Polymer droplets; Phase transition; Superspreading; Self-lubrication

Citation: Song, Y. Z.; Chen, X. C.; Liu, Y. J.; Wu, P. Y. Liquid crystal-driven superspreading of polymer droplets at the air-water interface. *Chinese J. Polym. Sci.* https://doi.org/10.1007/s10118-026-3756-9

INTRODUCTION

When a droplet falls on the water surface, it first stays briefly and then breaks, creating a smaller droplet that bounces off. This process was repeated several times until the droplet was completely dissolved in water.[1–3] In stark contrast, when a droplet of organic solvent falls onto the water surface, it spreads out like a pancake to form a layer of liquid film before completely dissolving in water.[4,5] This spreading depends on the difference in the surface tension between the organic solvent droplet and water. The surface tension of organic solvents is usually lower than that of water. Liquid spreading is of significant interest in science and technology, and has been widely used in interface science and materials science[6] particularly for fabricating thin polymer films with ordered structures.[7–9]

The fabrication of thin polymer films on solid substrates faces two major obstacles: maintaining the continuity and uniformity of the polymer films when the film thickness is reduced to the nanometer scale and achieving effective large-area separation and transfer processes. The key to forming a uniform and controllable liquid film on solid substrates is to suppress the hysteresis of the gas-liquid-solid three-phase contact line while spreading the polymer solutions.[10] By adjusting the wettability of the polymer solutions at the solid surface, it is possible to reduce the hysteresis of the three-phase contact line. Common strategies include creating multiscale structures on solid surfaces[11] and incorporating surfactants into polymer solutions.[12,13] However, the hysteresis of the three-phase contact line on the surface of solid materials is unavoidable. The spreading of polymer droplets on liquid substrates offers a distinct route for the fabrication of ultrathin films. Unlike solid substrates, where microscopic roughness, chemical heterogeneity, and no-slip boundary conditions generate contact-line pinning and hysteresis, water surfaces are molecularly smooth, deformable, and mobile.[14,15] It can largely circumvent the fixed gas-liquid-solid three-phase contact line encountered on solid supports. In addition, the high surface tension of water provides a driving force for the spread of organic droplets with low surface tension. However, replacing a solid substrate with a liquid one introduces a different dissipative factor. During the rapid spreading of polymer-containing droplets, relative motion,

* Corresponding authors, E-mail: liuyanjun@dhu.edu.cn (Y.J.L.)
E-mail: wupeiyi@dhu.edu.cn (P.Y.W.)
Special Issue: New Polymeric Supramolecular Substances
Received April 27, 2026; Accepted May 23, 2026; Published online August 19, 2026

deformation, and possible local slip can occur at the liquid-liquid interface, and these effects can limit the coherent expansion of the polymer film. Therefore, reducing this operational interfacial resistance is essential for extending liquid-supported spreading into large-area, transferable ultrathin polymer films.

Here, we present a simple and universal liquid-crystal-mediated superspreading approach for fabricating ultrathin polymer films by dropping polymer solutions containing liquid crystal 4-cyano-4′-heptylbiphenyl (7CB) onto a calcium chloride ($CaCl_2$) aqueous solution. The hydrophobic liquid crystal 7CB[16,17] acts as a molecular interfacial lubricant that enables rapid, large-area spreading of polymer droplets on a high-surface-tension aqueous substrate. Because the polymer/7CB solution is close to the nematic-isotropic transition temperature during deposition, 7CB reaches a low-mobility nematic liquid-crystalline state before or immediately during spreading. The 7CB molecules enriched near the organic side of the solvent-water interface form a lubricating interfacial region, which reduces the resistance to liquid-liquid relative motion, while the surface-tension difference provides the spreading driving force (Fig. 1a). This liquid driven superspreading strategy can be applied to elastic, elastoplastic, and plastic polymer materials. Additionally, liquid crystal 7CB can be removed on demand or utilized as a structural master to tailor the structures of ultrathin polymer films to achieve multifunctional integration. As a proof of concept, the *in situ* welding of silver nanowires (AgNWs) onto a 150-nm-thick EVA film by liquid crystal 7CB creates a conductance-stable elastic conductor for on-skin electronics. The elastic EVA conductor exhibited ultrathin thickness, high extensibility, strong tissue adhesion, water and gas permeability, biocompatibility, and stable conductivity.

EXPERIMENTAL

Materials

n-Hexane, tetrahydrofuran, toluene, ethanol, and calcium chloride ($CaCl_2$) were purchased from Greagent. Poly(ethylene-*co*-vinyl acetate) (EVA, vinyl acetate 32 wt%) and styrene ethylene butylene styrene (SEBS) were purchased from Macklin. Poly(vinylidene fluoride-*co*-trifluoroethylene) (P(VdF-TrFE)) was purchased from Sigma-Aldrich. AgNWs (5 mg·mL^{-1} dispersed in ethanol, diameter: 35–45 nm, length: 25–35 μm) were purchased from J&K. 4-Cyano-4′-n-heptylbiphenyl (7CB) was purchased from Meryer. All chemicals were used without further purification, and deionized (DI) water was used in all experiments.

Preparation of Ultrathin EVA Film, P(VdF-TrFE) Film and SEBS Film

One gram of polymer was dissolved in 10 mL of solvent con-

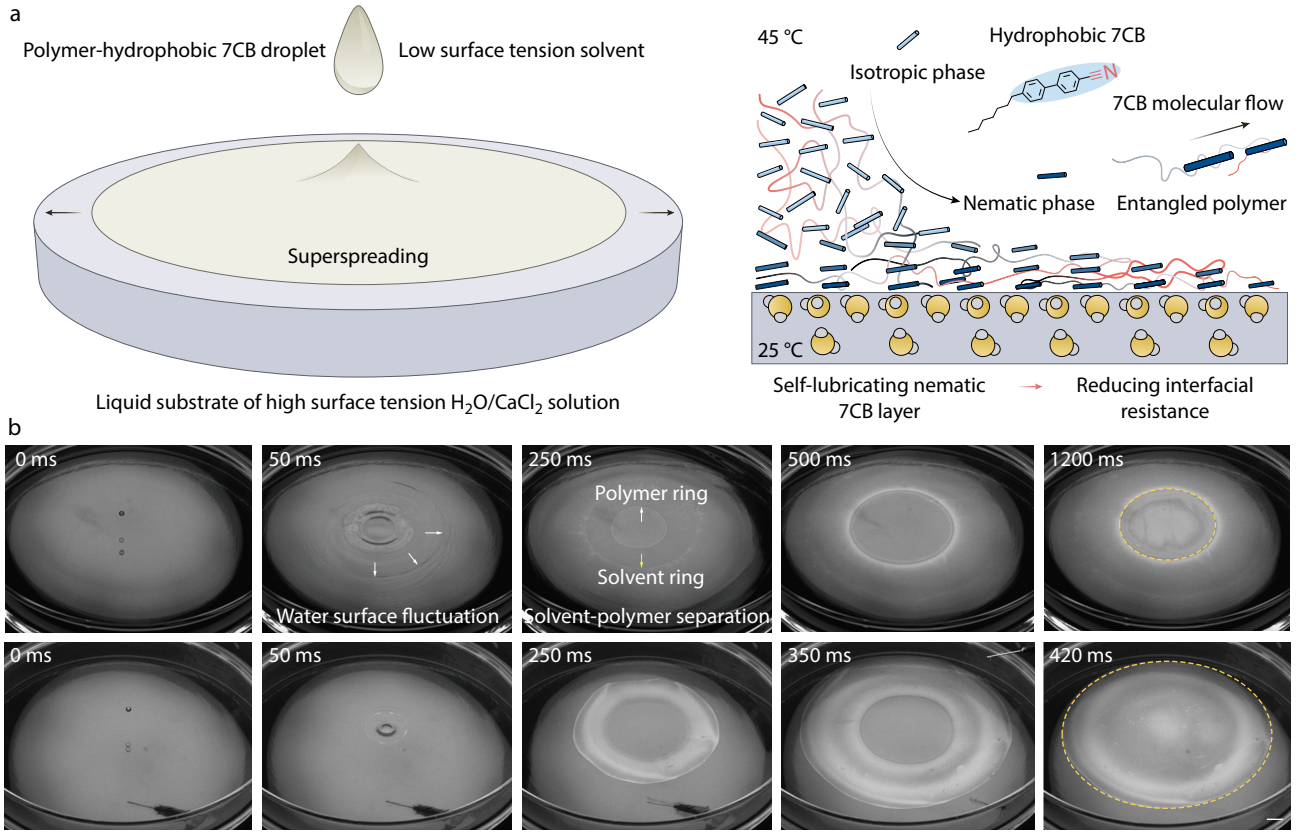

Fig. 1 (a) Schematics showing the superspreading process of a polymer droplet on the water surface mediated by hydrophobic 7CB. 7CB does not form a macroscopically separated pure layer; instead, 7CB remains mixed with the polymer/solvent phase in the bulk droplet while becoming enriched near the organic side of the droplet-water interface, where it forms a nematic 7CB-containing lubricating region. (b) Photographs showing the limited spreading process of an EVA droplet without 7CB (top) on the water surface and the enhanced superspreading process of an EVA-7CB droplet. Scale bar: 1 cm.

https://doi.org/10.1007/s10118-026-3756-9

taining 1 g of 7CB, and then stirred at 45 °C for 1 h. The solvents in the solution can be adjusted depending on the type of polymer. For example, 1 g of EVA, P(VdF-TrFE), and SEBS were dissolved in 10 mL of hexane, tetrahydrofuran, and toluene containing 1 g of 7CB, respectively. Using a 5-mL syringe, the polymer solution at 40 °C was dropped at the center of the container (diameter of 150 mm), which was filled with a high-surface-tension $CaCl_2$ solution (3.6 mol·L^{-1}). The droplet spontaneously spreads on the water surface to form a large liquid film. The free-standing ultrathin film was obtained by complete evaporation of the solvent and could be directly transferred to the next step.

Preparation of Ultrathin EVA Conductor

The as-prepared EVA film (E-film) was plasma-treated for 30 s and then placed flat on the DI water surface without submerging. A droplet of the AgNW solution was dripped onto the film and spontaneously spread into a uniform liquid layer. The droplet spontaneously spread across the film surface, forming a uniform liquid layer. Because ultrathin E-films are highly permeable to ethanol, the ethanol solvent permeates through the film into the water phase. Meanwhile, the silver nanowires were retained on the surface of the E-film and gradually accumulated to form a conductive network.

RESULTS AND DISCUSSION

Liquid Crystal-driven Superspreading

The surface tension of the EVA droplets (*n*-hexane as the solvent) was only 20.7 mN·m^{-1}. The surface tension of water at room temperature is 72.0 mN·m^{-1}. The EVA droplet was placed 5 cm above the water surface before it fell. The height of the liquid substrate is 10 cm. When an EVA droplet was dropped onto the water surface, the EVA droplet spontaneously spread to form an ultrathin EVA film (Fig. 1b). The time required for the EVA droplet to spread completely was 1200 ms. The impact of the EVA droplet caused the water surface to fluctuate violently, breaking the continuity of the tension difference between the EVA droplet and the air-water interface (the spreading process can be seen in Video S1 in the electronic supplementrary information, ESI). More importantly, the organic solvent and EVA separated during the spreading process, and the organic solvent exhibited a larger surface area. Owing to the limited tension difference and high interfacial resistance, the EVA droplet failed to achieve the optimal spreading area.

To increase the tension difference between the EVA droplet and the water surface, we enhanced the surface tension of water by adding $CaCl_2$. The experimental results indicate that the optimal concentration of $CaCl_2$ is 3.6 mol·L^{-1} (Fig. 2a), corresponding to a tension difference of 92.5 mN·m^{-1} between the EVA droplet and the $CaCl_2$ aqueous solution (Fig. 2b). We reduced the height of the liquid substrate to minimize the fluctuation amplitude of the water surface during droplet impact. The experimental results indicated that the optimal height of the liquid substrate is 2 cm (Fig. 2b). Although the tension difference was optimized to the maximum and the water surface fluctuation was minimized, the spreading area of the EVA droplet was still not ideal, measuring only approximately 8 cm in diameter. Under these optimized conditions, the remaining limitation cannot be attributed to insufficient surface-tension differences or macroscopic water surface fluctuations. Therefore, we used interfacial resistance in an operational sense to describe the dissipative resistance associated with relative motion, deformation, and possible local slip at the polymer/solvent droplet-water interface during rapid spreading.

To reduce the interfacial resistance of the EVA droplets during the spreading process, we created a self-lubricating layer between the surface of the EVA droplet and $CaCl_2$ aqueous solution by adding hydrophobic liquid crystal 7CB to the EVA droplet. When an EVA droplet containing liquid crystal 7CB (EVA-7CB droplet) was dropped onto the water surface, the EVA-7CB droplet spontaneously spread to form an ultrathin EVA film with a diameter of 13 cm (Fig. 1b; the spreading process is shown in Video S2 in ESI). The time required for the EVA-7CB droplet to spread completely was 420 ms. Notably, the organic solvent and EVA did not separate during the spreading process, indicating that their spreading rates remained consistent. The comparison between the EVA and EVA-7CB droplets provides direct evidence of reduced operational interfacial resistance. Under otherwise comparable conditions, adding 7CB increases the spreading diameter from approximately 8 cm to 13 cm, shortens the spreading time from approximately 1200 ms to 420 ms, and suppresses solvent-polymer separation. These changes indicate that 7CB facilitates coherent liquid-liquid spreading by reducing the resistance at the moving droplet-water boundary.[18] The spread area and efficiency surpass those of existing natural and artificial spreading methods.[9,10,19–22] With an increase in the content of liquid crystal 7CB at the same temperature and tension difference, the superspreading areas of the EVA films gradually increased, confirming the positive effect of liquid crystal 7CB on the superspreading process (Fig. 2b). The experimental results indicate that the optimal 7CB content is equal to the mass of the EVA. If the 7CB content exceeds that of the EVA, visible perforation defects could occur in the superspreading membranes because of excessive 7CB breaking the polymeric continuity.

In this work, normal spreading without 7CB is slow, yields a small final area, and involves solvent-polymer separation. In contrast, superspreading with 7CB is fast, taking approximately 420 ms, producing a large continuous film of approximately 13 cm in diameter, suppressing solvent-polymer separation, and forming a transferable ultrathin film.

Self-lubricating Interfacial Layer of Liquid Crystals

The hydrophobicity of 7CB was determined by contact angle and sliding angle measurements. As shown in Fig. 2(c), the pure EVA film exhibited contact and sliding angles of 78° and 35°, respectively. After the addition of 7CB, the contact angle of the EVA film increased to 84.5°, whereas the sliding angle decreased to 12°. These changes indicated 7CB-associated surface enrichment and reduced resistance to interfacial motion. Because 7CB is hydrophobic and remains soluble in organic/polymer-rich droplets, it is not expected to migrate into the $CaCl_2$ aqueous phase. Instead, 7CB preferentially localizes on the organic side of the solvent-water interface, where it partially replaces direct contact between the polymer/solvent phase and water, thereby lowering the interfacial free energy. This interfacial enrichment provided a thermodynamic basis for the forma-

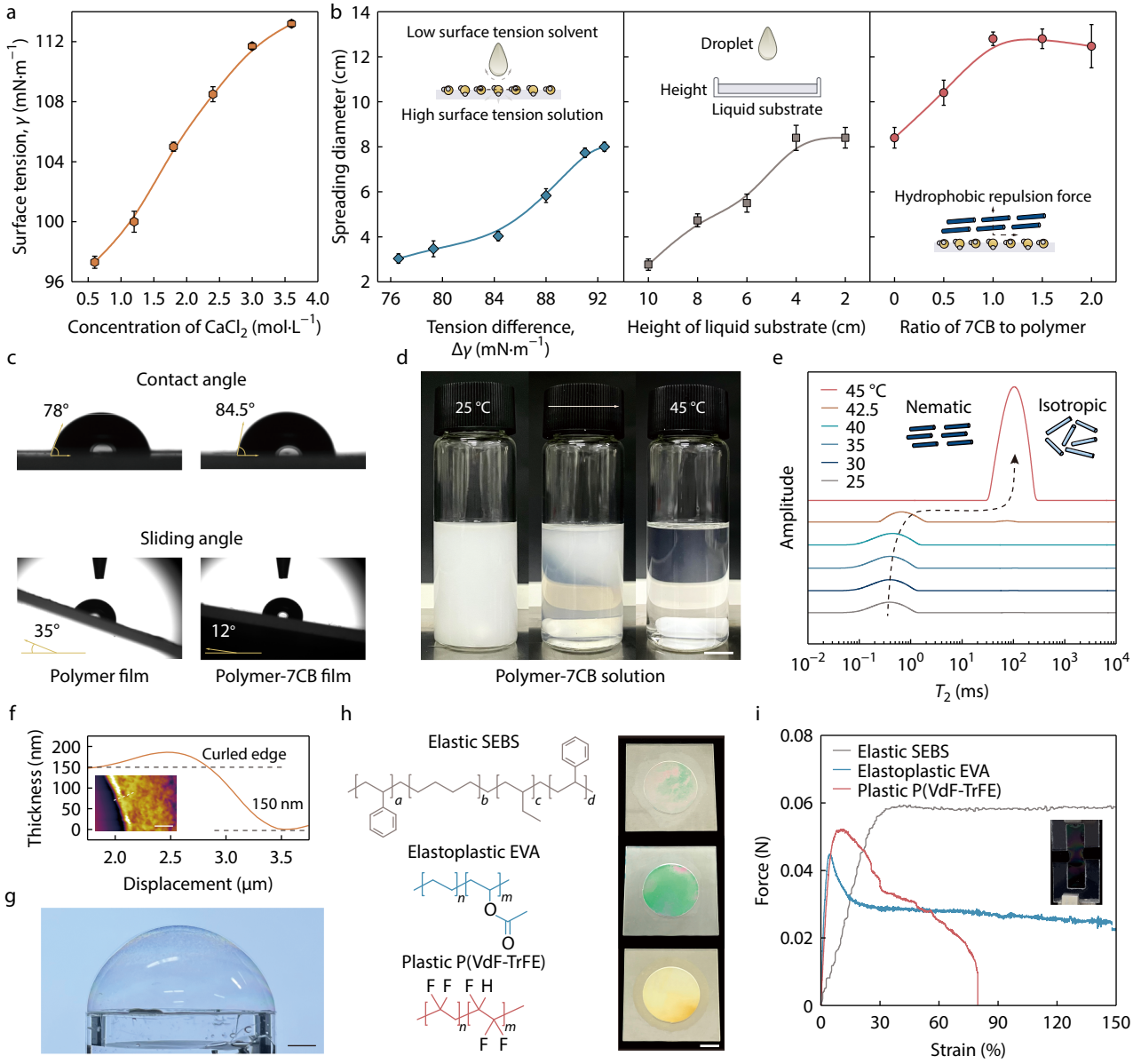

Fig. 2 (a) The surface tension of the liquid substrate as a function of the concentration of $CaCl_2$; (b) The effect of the tension difference between the EVA droplet and the liquid substrate, the height of the liquid substrate, and the ratio of 7CB to EVA on the spreading diameter of EVA droplets; (c) The contact angle and sliding angle of water droplets on EVA film and EVA-7CB film; (d) Photographs showing the phase transition process of 7CB from nematic to isotropic in the EVA-7CB mixed solution from 25 °C to 45 °C (*n*-hexane as the solvent. Scale bar: 1 cm); (e) T_2 time change of the EVA-7CB mixed solution from 25 °C to 45 °C measured by low-field ^{1}H-NMR; (f) The thickness of superspreading EVA film. Inset: AFM image of the superspreading EVA film, scale bar: 2 μm; (g) Photograph showing the expansion in volume of a 150-nm-thick ultrathin EVA film after being inflated. Scale bar: 1 cm; (h) Structural formulas for elastic SEBS, elastoplastic EVA and plastic P(VdF-TrFE). Photographs of ultrathin SEBS film, EVA film and P(VdF-TrFE) film. Scale bar: 1 cm; (i) Force-strain curves of the ultrathin SEBS, EVA, and P(VdF-TrFE) films.

tion of a 7CB-containing lubricating region during rapid spreading. The molecular dynamics of liquid crystal 7CB during the superspreading process were elucidated using low-field nuclear magnetic resonance (NMR). 7CB is a typical thermotropic liquid crystal (LC).[23] Optical images of the EVA-7CB solution showed a sharp phase transition process as the temperature increased from 25 °C to 45 °C (Fig. 2d). To accurately characterize the phase transition temperature of liquid crystal 7CB,[24] we utilized low-field NMR to measure the transverse relaxation (T_2) time of the EVA-7CB solution at various temperatures. The low-field NMR spectra indicate that the phase transition temperature of 7CB is 42.5 °C (Fig. 2e). Below 42.5 °C, the T_2 time of the EVA-7CB solution is only 0.3 ms, indicating that 7CB is in a low-mobility nematic liquid-crystalline state. This liquid-crystalline ordering was further supported by POM. As shown in Fig. S1 (in ESI), the ultrathin EVA-7CB film exhibits clear birefringence, confirming the presence of ordered liquid crystalline domains. When the temperature increased to 45 °C, the T_2 time increased to 114 ms, indicating that 7CB transitioned into a highly mobile isotropic state. When the temperature increased to 45 °C, the T_2

time of the EVA-7CB solution increased to 114 ms, indicating that 7CB transitions into a highly active isotropic phase. The temperature dynamics during droplet deposition further clarified when the nematic state was established. Because the polymer/7CB solution is delivered at 40 °C, which is close to or slightly below the clearing temperature measured by low-field NMR, 7CB can reach a nematic, low-mobility state before or immediately during spreading. Infrared thermal imaging further showed that the droplet cooled rapidly during the deposition. Under lower thermal-contrast conditions, the droplet temperature decreased by approximately 2–3 °C within the first 200 ms after contact with the aqueous substrate, confirming rapid quenching by the water bath (Video S3 in ESI). Such rapid cooling promotes the formation of a 7CB-containing nematic lubricating region, while suppressing large-scale phase separation.

We also examined the spreading behavior of $CaCl_2$ aqueous substrates at different temperatures. The spreading diameter increased as the substrate temperature increased from 25 °C to 55 °C (Fig. S2 in ESI). Temperature alters the surface tension and viscosity of the droplet, solvent evaporation, and spreading driving force. Thus, superspreading is a coupled process: the surface-tension difference drives spreading, while interfacially enriched 7CB reduces the resistance to coherent liquid-liquid motion.

Ultrathin Polymer Films for Bioelectronic Applications

Despite being only 150 nm thick (Fig. 2f), the EVA film could be easily detached from the water surface and transferred to various substrates, such as wafers, plastic substrates, and other ultrathin polymer films. To verify uniformity across the entire film, AFM measurements were performed at the center, middle, and edge positions (Fig. S3 in ESI). The measured thicknesses at these positions remained close to 150 nm, confirming that the superspreading process produced a highly uniform ultrathin film over a large-area water surface. Moreover, the ultrathin EVA film maintained its integrity when subjected to large biaxial strain, showing high extensibility (Fig. 2g). In addition to the elastoplastic EVA, the liquid-crystal-mediated superspreading strategy is generally applicable to elastic SEBS and plastic P(VdF-TrFE) (Fig. 2h). These ultrathin polymer films exhibit uniform thickness and surface structure, as evidenced by their consistent interference color when viewed from a specific angle. These ultrathin polymer films were self-supporting and exhibited excellent mechanical properties. The ultrathin SEBS film was highly elastic with a strain rate exceeding 150% (Fig. 2i). The ultrathin EVA film exhibited clear yielding characteristics with a strain rate exceeding 150%. Although the P(VdF-TrFE) film had plastic properties, its strain rate still reached 70%.

Importantly, liquid crystal 7CB can be selectively removed after completing the mission of molecular interface lubrication or can be utilized as a structural master to tailor the structures of ultrathin polymer films to achieve multifunctional integration. The 7CB was dissolved in ethanol.[25] As a proof of concept, a droplet of an ethanol solution containing AgNWs was dropped onto the ultrathin EVA film to integrate multiple functions.

The AgNW–ethanol solution spread on the surface of the ultrathin EVA film, causing liquid crystal 7CB to precipitate from inside the ultrathin EVA film and weld the AgNWs *in situ* (Fig. 3a). The Laplace pressure difference[26] induced aggregation of 7CB at the intersection of the AgNWs upon ethanol evaporation. This phenomenon enables the *in situ* welding of AgNWs on ultrathin EVA films, resulting in ultrathin elastic conductors. The transparency of the ultrathin EVA film did not decrease with the addition of AgNWs; in fact, it increased

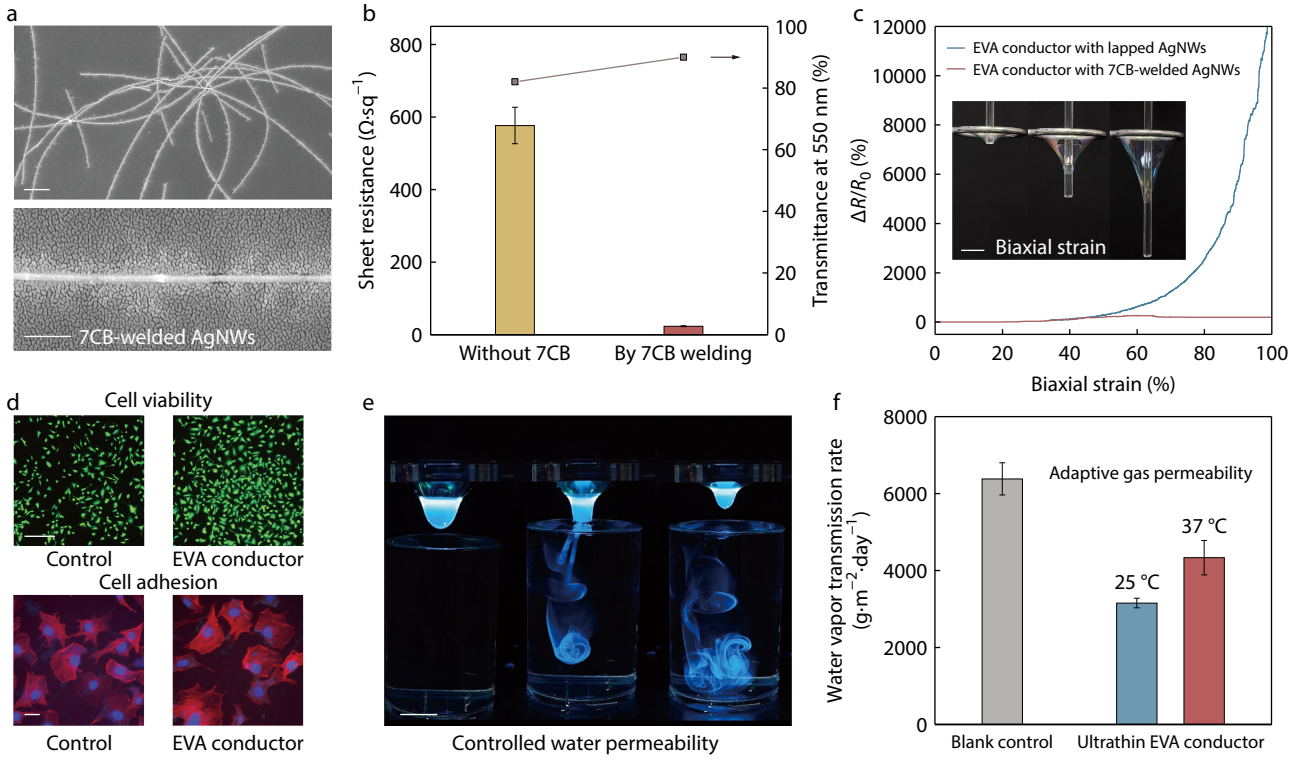

https://doi.org/10.1007/s10118-026-3756-9

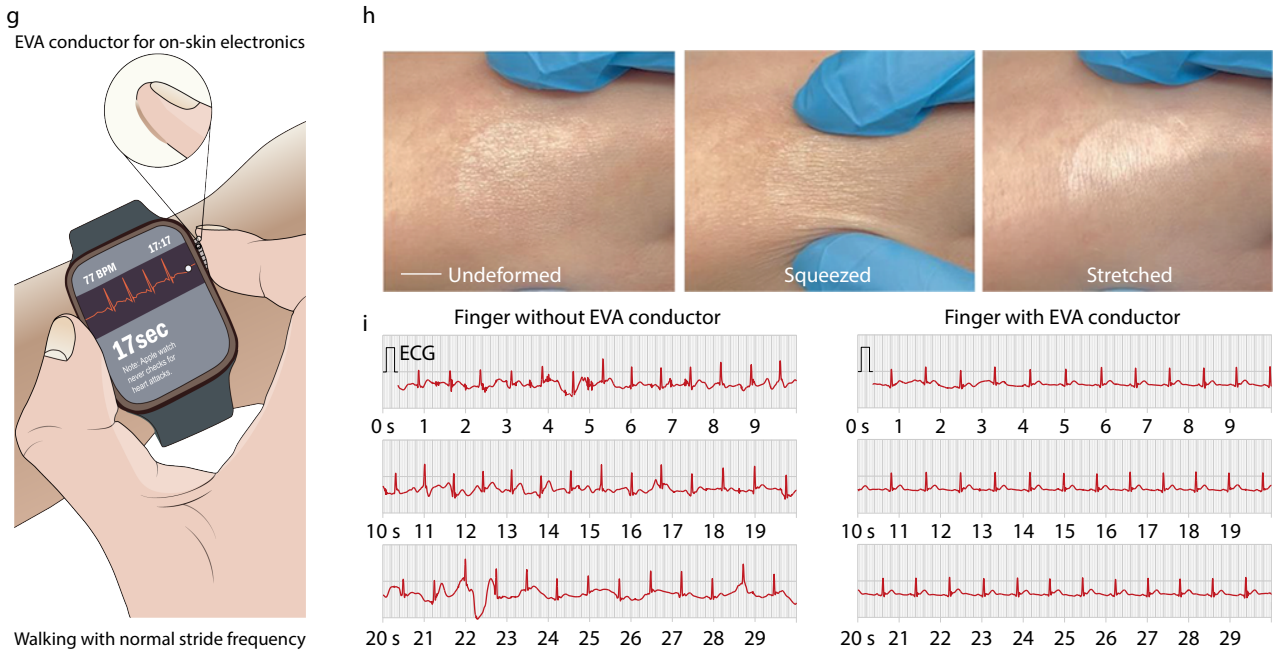

Fig. 3 (a) SEM image of the ultrathin EVA film with 7CB-welded AgNW networks and magnified SEM image of an AgNW that was welded to the ultrathin EVA film using 7CB, scale bars: 2 μm (top) and 200 nm (down); (b) The sheet resistance and transparency of the ultrathin EVA conductor without 7CB and the ultrathin EVA conductor with 7CB-welded AgNW networks; (c) The resistance change of the ultrathin EVA conductor with lapped AgNW networks and the ultrathin EVA conductor with 7CB-welded AgNW networks during biaxial strain. Inset: the biaxial strain of the ultrathin EVA conductor, scale bar: 1cm; (d) Fluorescence images of stained human umbilical vein endothelial cells cultured on control materials (polyethylene terephthalate substrate for viability and 96-well plates for adhesion) as well as on the ultrathin EVA conductor for 24 h. Microfilament (red) and nuclei (blue). Scale bars: 500 μm (top) and 200 μm (down). (e) Photographs showing the water permeability of the ultrathin EVA conductor (fluorescent in the water solution, under UV light), scale bar: 1 cm; (f) The gas permeability of the ultrathin EVA conductor at 25 and 37 °C; (g) Schematics of the ultrathin EVA conductor as a human-computer interaction interface for detecting the ECG of a person walking at a normal pace; (h) Photographs of the ultrathin EVA conductor attached conformally to human skin, scale bar: 1 cm; (i) Comparison of ECG signals monitored by direct contact with the finger and *via* the EVA conductor.

slightly (Fig. 3b). The sheet resistance of the 7CB-welded AgNW networks was 25 times lower than that of the commonly lapped AgNW networks. Furthermore, the ultrathin EVA conductor with 7CB-welded AgNWs exhibited strain-insensitive conductivity (Fig. 3c). When the ultrathin EVA conductor was stretched to 100% of its original area, the resistance of the conductor with 7CB-welded AgNW networks showed a slight increase. In comparison, the resistance of the ultrathin EVA conductor with lapped AgNW networks increased significantly by 12000%.

The human umbilical vein endothelial cells demonstrated robust adhesion and spreading behavior when cultured on the surface of the ultrathin EVA conductor (Fig. 3d). The favorable morphology and activity observed in these cells suggest that the ultrathin EVA conductor is noncytotoxic and biocompatible. The ultrathin EVA conductor allowed water to pass through when its bottom came into contact with the water surface, indicating controlled permeability (Fig. 3e, water permeability can be seen in Video S4 in ESI). As the temperature increased from 25 °C to 37 °C (body temperature), the water vapor transmission rate of the bottle sealed by the ultrathin EVA conductor significantly increased (Fig. 3f), indicating adaptive gas permeability. The combination of these properties, along with the natural ability of the nanometer-scale film to conform to human skin, allows this ultrathin EVA conductor to be used in seamless on-skin electronics (Figs. 3g and 3h). Owing to the high damping properties of EVA materials[27] and the strain-insensitive conductivity of 7CB-welded AgNW networks, the ultrathin EVA conductor can effectively suppress motion artifacts caused by interface impedance instability when monitoring a human electrocardiogram (ECG), thereby obtaining clear ECG signals (Fig. 3i).

CONCLUSIONS

In this work, we developed a facile and universally applicable liquid-crystal-mediated superspreading strategy for fabricating ultrathin polymer films using elastic, elastoplastic, and plastic polymer materials. The hydrophobic liquid crystal 7CB acts as a molecular interface lubricant to enable rapid, large-area superspreading of polymer droplets on the water surface with high surface tension. During deposition, 7CB reaches a low-mobility nematic liquid-crystalline state and becomes enriched near the organic side of the solvent-water interface, forming a 7CB-containing lubricating region that reduces resistance to coherent liquid-liquid spreading. Importantly, liquid crystal 7CB can be selectively removed after completing the mission of molecular interface lubrication or can be utilized as a structural master to tailor the structures of ultrathin polymer films to achieve multifunctional integration. The combination of high extensibility, strong tissue adhesion, water and gas permeability, biocompatibility, and stable conductivity makes this ultrathin EVA conduc-

tor ideal for use in seamless on-skin electronics as a proof of concept.

Conflict of Interests

The authors declare no interest conflict.

Electronic Supplementary Information

Electronic supplementary information (ESI) is available free of charge in the online version of this article at http://doi.org/10.1007/s10118-026-3756-9.

Data Availability Statement

The related data of this paper is data that should not be shared, and can be obtained from the author for reasonable reasons. The author's contact information: liuyanjun@dhu.edu.cn.

ACKNOWLEDGMENTS

This work was financially supported by the National Natural Science Foundation of China (Nos. 52433003 and 22405038) and Fundamental Research Funds for the Central Universities (No. 2232026D27).

REFERENCES

1 Couder, Y.; Fort, E.; Gautier, C. H.; Boudaoud, A. From bouncing to floating: noncoalescence of drops on a fluid bath. *Phys. Rev. Lett.* **2005**, *94*, 177801.
2 Couder, Y.; Protière, S.; Fort, E.; Boudaoud, A. Walking and orbiting droplets. *Nature* **2005**, *437*, 208–208.
3 Schutzius, T. M.; Jung, S.; Maitra, T.; Graeber, G.; Köhme, M.; Poulikakos, D. Spontaneous droplet trampolining on rigid superhydrophobic surfaces. *Nature* **2015**, *527*, 82–85.
4 Kim, H.; Muller, K.; Shardt, O.; Afkhami, S.; Stone, H. A. Solutal Marangoni flows of miscible liquids drive transport without surface contamination. *Nat. Phys.* **2017**, *13*, 1105–1110.
5 Jung, D.; Lim, C.; Shim, H. J.; Kim, Y.; Park, C.; Jung, J.; Han, S. I.; Sunwoo, S.-H.; Cho, K. W.; Cha, G. D.; Kim, D. C.; Koo, J. H.; Kim, J. H.; Hyeon, T.; Kim, D.-H. Highly conductive and elastic nanomembrane for skin electronics. *Science* **2021**, *373*, 1022–1026.
6 Dai, Y.; Li, M.; Ji, B.; Wang, X.; Yang, S.; Yu, P.; Wang, S.; Hao, C.; Wang, Z. Liquid metal droplets bouncing higher on thicker water layer. *Nat. Commun.* **2023**, *14*, 3532.
7 Zhang, P.; Zhang, F.; Zhao, C.; Wang, S.; Liu, M.; Jiang, L. Superspreading on immersed gel surfaces for the confined synthesis of thin polymer films. *Angew. Chem. Int. Ed.* **2016**, *55*, 3615–3619.
8 Zhou, T.; Zhao, C.; Liu, Y.; Huang, J.; Zhou, H.; Nie, Z.; Fan, M.; Zhao, T.; Cheng, Q.; Liu, M. Large-area ultrastrong and stiff layered MXene nanocomposites by shear-flow-induced alignment of nanosheets. *ACS Nano* **2022**, *16*, 12013–12023.
9 Tang, S.; Gong, J.; Shi, Y.; Wen, S.; Zhao, Q. Spontaneous water-on-water spreading of polyelectrolyte membranes inspired by skin formation. *Nat. Commun.* **2022**, *13*, 3227.
10 Zhao, C.; Zhang, P.; Zhou, J.; Qi, S.; Yamauchi, Y.; Shi, R.; Fang, R.; Ishida, Y.; Wang, S.; Tomsia, A. P.; Liu, M.; Jiang, L. Layered nanocomposites by shear-flow-induced alignment of nanosheets. *Nature* **2020**, *580*, 210–215.
11 Sun, Z.; Zeng, X.; Deng, X.; Zhang, X.; Zhang, Y. Droplet interface in additive manufacturing: from process to application. *Droplet* **2023**, *2*, e57.
12 Sun, S.; Li, S.; Feng, W.; Luo, J.; Russell, T. P.; Shi, S. Reconfigurable droplet networks. *Nat. Commun.* **2024**, *15*, 1058.
13 Liu, X.; Shi, S.; Li, Y.; Forth, J.; Wang, D.; Russell, T. P. Liquid tubule formation and stabilization using cellulose nanocrystal

Graphical Abstract

Liquid Crystal-driven Superspreading of Polymer Droplets at the Air-Water Interface

Yuan-Zhu Song, Xing-Chao Chen, Yan-Jun Liu, and Pei-Yi Wu

Donghua University

During droplet spreading, the hydrophobic liquid crystal 4-cyano-4′-heptylbiphenyl (7CB) undergoes an isotropic-to-nematic transition, forming a self-lubricating interface that enables polymer droplets to rapidly spread into transferable ultrathin nanofilms.

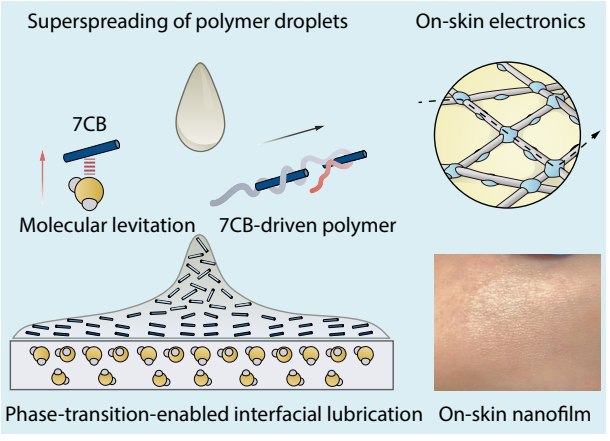

Chinese J. Polym. Sci., 2026 *https://doi.org/10.1007/s10118-026-3756-9*

surfactants. *Angew. Chem. Int. Ed.* **2017**, *56*, 12594–12598.
14 Smit, W. J.; Bakker, H. J. The surface of ice is like supercooled liquid water. *Angew. Chem. Int. Ed.* **2017**, *56*, 15540–15544.
15 Stiopkin, I. V.; Weeraman, C.; Pieniazek, P. A.; Shalhout, F. Y.; Skinner, J. L.; Benderskii, A. V. Hydrogen bonding at the water surface revealed by isotopic dilution spectroscopy. *Nature* **2011**, *474*, 192–195.
16 Rather, A. M.; Xu, Y.; Chang, Y.; Dupont, R. L.; Borbora, A.; Kara, U. I.; Fang, J. C.; Mamtani, R.; Zhang, M.; Yao, Y.; Adera, S.; Bao, X.; Manna, U.; Wang, X. Stimuli-responsive liquid-crystal-infused porous surfaces for manipulation of underwater gas bubble transport and adhesion. *Adv. Mater.* **2022**, *34*, 2110085.
17 Xu, Y.; Chang, Y.; Yao, Y.; Zhang, M.; Dupont, R. L.; Rather, A. M.; Bao, X.; Wang, X. Modularizable liquid-crystal-based open surfaces enable programmable chemical transport and feeding using liquid droplets. *Adv. Mater.* **2022**, *34*, 2108788.
18 Tadokoro, C.; Nihira, T.; Nakano, K. Minimization of friction at various speeds using autonomous viscosity control of nematic liquid crystal. *Tribol. Lett.* **2014**, *56*, 239–247.
19 Zheng, S.; Du, M.; Miao, W.; Wang, D.; Zhu, Z.; Tian, Y.; Jiang, L. 2D prior spreading inspired from Chinese Xuan papers. *Adv. Funct. Mater.* **2018,** *28*, 1800832.
20 Miao, W.; Zheng, S.; Zhou, J.; Zhang, B.; Fang, R.; Hao, D.; Sun, L.; Wang, D.; Zhu, Z.; Jin, X.; Tian, Y.; Jiang, L. Microchannel and nanofiber array morphology enhanced rapid superspreading on animals' corneas. *Adv. Mater.* **2021**, *33*, 2007152.
21 Zhu, Z.; Tian, Y.; Chen, Y.; Gu, Z.; Wang, S.; Jiang, L. Superamphiphilic silicon wafer surfaces and applications for uniform polymer film fabrication. *Angew. Chem. Int. Ed.* **2017**, *56*, 5720–5724.
22 Zhu, Z.; Chen, Y.; Luo, X.; Miao, W.; Dong, Z.; Zhou, J.; Tian, Y.; Jiang, L. Ultrafast impact superspreading on superamphiphilic silicon surfaces for effective thermal management. *J. Am. Chem. Soc.* **2023**, *145*, 15128–15136.
23 Ojha, D. P.; Praveen, P. L. Theoretical study on liquid crystal cyanobiphenyls: phase stability and phase behavior. *J. Phys. Chem. Solids* **2013**, *74*, 1653–1659.
24 Liu, Y.; Zhang, J.; Wu, P. Near-frictionless long-distance water transport in trees enabled by hierarchically helical molecular pumps. *CCS Chem.* **2025**, *7*, 484–492.
25 Zhang, X.; Liu, X.; Zhang, X.; Tian, Y.; Meng, Y. Ordering of the 7CB liquid crystal induced by nanoscale confinement and boundary lubrication. *Liq. Cryst.* **2012**, *39*, 1305–1313.
26 Dai, H.; Dong, Z.; Jiang, L. Directional liquid dynamics of interfaces with superwettability. *Sci. Adv.* **2020**, *6*, eabb5528.
27 Liu, Y.; Zhang, J.; Wu, P. Hierarchically structured bioinspired fibers shaped by liquid droplets. *Adv. Funct. Mater.* **2024**, *34*, 2311704.

https://doi.org/10.1007/s10118-026-3756-9